Journal of Catalysis 355 (2017) 131–138

Contents lists available at ScienceDirect

Journal of Catalysis

journal homepage: www.elsevier.com/locate/jcat

Defect porous organic frameworks (dPOFs) as a platform for chiral organocatalysis

Zu-Jin Lin [a,b], Jian Lü [a], Lan Li [a], Hong-Fang Li [a], Rong Cao [a,*]

[a] State Key Laboratory of Structural Chemistry, Fujian Institute of Research on the Structure of Matter, Chinese Academy of Sciences, Fuzhou 350002, PR China
[b] Department of Applied Chemistry, College of Life Science, Fujian Agriculture and Forestry University, Fuzhou, Fujian 350002, PR China

ARTICLE INFO

Article history:
Received 20 April 2017
Revised 13 September 2017
Accepted 18 September 2017

Keywords:
Defect porous organic frameworks (dPOFs)
Heterogeneous catalysis
Aldol reaction
Asymmetric catalysis
Porous organic polymers (POPs)

ABSTRACT

Porous organic frameworks (POFs) are emerging as an important class of porous materials. The absence of functional groups in POFs, however, renders them relatively nonspecific as porous materials for applications such as in heterogeneous chiral catalysis. Although pre- and post-synthetic modifications have been developed for the functionalization of POFs, the introduction of functional groups into POFs remains a great challenge. Herein we have advanced a facile and versatile strategy to uniformly incorporate targeted functional groups into defect porous organic frameworks (dPOFs) by one-pot copolymerization of low-connected functional and primitive multi-connected building blocks. Based on this strategy, four proline-functionalized dPOFs were readily synthesized and developed as new platforms for heterogeneous chiral organocatalysis. The as-prepared dPOFs show higher catalytic activity and superior enantioselectivity than that of their homogeneous counterpart L-proline in the catalytic direct aldol reaction between 4-nitrobenzaldehyde and acetone, and could be reused at least five times without significant loss of catalytic activity and enantioselectivity.

1. Introduction

Porous organic frameworks (POFs) have emerged as a new generation of porous materials. Unlike porous inorganic materials and porous inorganic-organic materials, POFs are usually synthesized by the self- or cross-condensation of multi-connected organic building blocks, and are thus composed of organic moieties linked through strong covalent bonds [1,2]. The rich variety of organic building blocks combined with the diverse polymerization reactions has led to various types of novel POFs, including crystalline covalent organic frameworks (COFs) [3–5], hypercrosslinked polymers [6], covalent triazine-based frameworks (CTFs) [7], conjugated microporous polymers (CMPs) [8], polymers of intrinsic microporosity (PIMs) [9], porous aromatic frameworks (PAFs) [10], and porous polymers networks (PPNs) [11]. From a topological point view, the underlying topologies of the POFs that are currently available only belong to a few types of topological nets, including a 1D *quasiregular* **chain**, 2D **hcb**, **sql**, **gra**, **bnn** and 3D **ctn**, **bor**, **dia**, **aco**, and **lta** [12]. Given that the underlying topology plays a guiding role in the cross-linking of multi-connected organic building blocks, POF design becomes a judicious selection of appropriate multi-connected organic building blocks for the construction of the aforementioned topological nets. In this context, symmetric multi-connected (3-, 4- and 6-c) organic building blocks with special spatial conformation have been extensively applied in the construction of POFs [2,13]. At the same time, POFs have shown impressive applications in gas storage and separation and heterogeneous catalysis. The absence of functional groups such as catalytic sites, however, renders POFs relatively nonspecific as porous materials for applications such as heterogeneous catalysis and others. A facile and viable approach to incorporate targeted functional groups into POFs will greatly expand the applications of POFs.

Recently, two strategies, pre- and post-synthetic modification (PSM) methods were developed to functionalize POFs. The former approach relies on the pre-design and synthesis of multi-connected molecular building blocks with desired functional groups [14,15], and the latter depends on the synthesis of starting building blocks bearing the reactive species such as alkynes [16], hydroxyls [17,18], azides [19] or amines [20,21] for further post-modification. Therefore, both of them might suffer from limitations such as requirement of drastic synthesis conditions, tedious purification processes, and multistep synthesis during the syntheses of pre-designed multi-connected organic building blocks. More importantly, the pore sizes of the modified POFs are unavoidably significantly reduced in comparison to those of the pristine POFs

* Corresponding author.
E-mail address: rcao@fjirsm.ac.cn (R. Cao).

https://doi.org/10.1016/j.jcat.2017.09.014
0021-9517/

due to the ligating functional groups pointing toward the pores. This often results in significant reductions in both the accessibility of functional groups and the efficiency of mass-transport process, with concomitant tremendous detriment to POF performances in such as heterogeneous catalysis. Thus, to functionalize a POF by the introduction of targeted functional groups into pores, one should first consider the effects of the embedded functional groups. They have a dual role: they may endow the new functions to a POF, but they can also block the pores. A good balance between these dual roles in a POF would truly extend their applications in host-guest chemistry or heterogeneous catalysis.

In nature, "ideal structure", with an infinite periodic repetition of identical groups of atoms in space doesn't exist, even in crystalline materials. For example, MOFs, one of a typical crystalline materials, many of them are known to contain defects [22]. Intriguingly, defects in MOFs can be engineered to tune the physical-chemical properties of MOFs, opening up new avenues for their practical application [23,24]. For instance, through co-assembling of metal ions, ligands, and functional ligand-fragments (denoted as "metal-ligand-fragment coassembly strategy" in the original article), Zhou et al. have successfully introduced both the functional groups and mesoporous into a microporous MOF while preserved the MOF parent structure [25]. Inspired by the engineering defects in MOFs, herein, we report a facile and versatile strategy to construct defect porous organic frameworks (dPOFs, the structure is "defect" as compared to that of parent POFs from a topological view) with uniform decoration by accessible targeted functional groups through the one-fell-swoop copolymerization of an appropriate ratio of low-connected functional building blocks and primitive multi-connected ones in the *de novo* synthesis. The dual roles of functional groups can be well balanced *via* tuning the feeding ratios of the initial building blocks. The new procedure for the synthesis of the functional dPOFs may greatly extend the applications of POFs since the low-connected, especially for 1- and 2- connected functional building blocks, are often readily available or easily prepared. Based on this strategy, four proline-functionalized dPOFs (**dPOF-1**–**4**) were rationally designed and utilized as heterogeneous organocatalysts for the catalytic direct asymmetric aldol reactions. Remarkably, the as-synthesized dPOFs show both higher catalytic activity and better enantioselectivity than that of their homogeneous counterpart L-proline in the direct asymmetric aldol reaction between *p*-nitrobenzaldehyde and acetone, and these catalysts could be reused for at least five times in a role without significant loss of catalytic activity.

2. Materials and methods

2.1. General

N,N-dimethylformamide (DMF), tetrahydrofuran (THF), 1,5-cyclooctadiene (COD), and acetone were degassed before use. All reactions involving moisture sensitive reactants were performed under a nitrogen atmosphere using oven dried glassware. Anhydrous methanol, anhydrous dichloromethane (DCM), *Boc*-L-proline, 4-dimethylaminopyridine (DAMP), N,N′-dicyclohexylcarbodiimide (DCC), and trifluoroacetic acid (TFA) were purchased from J&K Scientific Ltd. 2,2′-bipyridyl, and bis(1,5-cyclooctadiene)nickel (0) [$Ni(COD)_2$] were purchased from Alfa Aesar. Tetrakis(4-bromophenyl)methane (**Br_4tpm**) and **PAF-1** was synthesized according to literature [10,26]. The synthetic procedures of (*S*)-*tert*-butyl-2-(2,5-dibromophenylsulfonylcarbamoyl)pyrrolidine-1-carboxylate (**Br_2-L_1-*Boc***), (*S*)-N-(2,5-dibromophenylsulfonyl)pyrrolidine-2-carboxamide (**Br_2-L_1**) and (*S*)-*tert*-butyl 2-(2-bromophenylsulfonylcarbamoyl)pyrrolidine-1-carboxylate (**Br-L_2-*Boc***) were shown in supporting information in detail. All other solvents, reagents and chemicals were purchased from Aladdin Industrial Corporation and used directly unless stated otherwise.

Thin-layer chromatography (TLC) plates were visualized by exposure to ultraviolet light. Flash column chromatography was carried out with silica gel (300–400 mesh). Nuclear magnetic resonance (NMR) spectra were recorded at ambient temperature on a BRUKER AVANCE III spectrometer, where the chemical shifts (δ in ppm) were referenced to a residual proton of the solvent as standard. Fourier transform infrared (IR) spectra were recorded on PerkinElmer Spectrum One as KBr pellets in the range 4000–400 cm^{-1}. Elemental analyses (C, H, N, and S) were carried out on an Elementar Vario EL III analyzer. Thermogravimetric analyses (TGA) were performed under N_2 atmosphere on an SDT Q600 thermogravimetric analyzer, with a heating rate of 10 °C min^{-1}. Powder X-ray diffraction (PXRD) data were recorded on a Rigaku MiniFlex2 diffractometer working with Cu Kα radiation, and the recording speed was 1° min^{-1} over the 2θ range of 5–50° at room temperature. Scanning electron microscopy (SEM) images were carried out on a SU-8010. High resolution transmission electron microscope (HRTEM) images were taken on a FEI TECNAI G2 F20 microscope at an accelerating voltage of 220 kV. Nitrogen sorption isotherms were measured at 77 K using a Micrometrics ASAP 2020 surface area and pore size analyzer. The Brunauer-Emmett-Teller (BET) method was utilized to calculate the specific surface areas. Pore size distribution data were calculated from the N_2 sorption isotherms based on the DFT model in the Micrometrics ASAP 2020 software package (assuming slit pore geometry). Prior to the measurements, the samples were degassed at 80 °C for 10 h. The solid-state NMR spectra were measured on a Bruker AVANCE 400 spectrometer using densely packed powders of the samples in 4 mm ZrO_2 rotors spinning at 12 kHz rate. High performance liquid chromatography was performed on a HITACHI L-2000 with Daicel chiral AD-H and AS-H columns with *i*-PrOH/*n*-hexane as the eluent.

2.2. Synthesis of dPOF-1–4

A mixture of **Br_2-L_1-*Boc*** (*x* mmol%, *x* = 25, 50 and 75) and tetrakis(4-bromophenyl)methane (**Br_4tpm**, (100-*x*) mmol%, total of 1 mmol) was added to a solution of 2, 2′-bipyridyl (936 mg, 6 mmol, 1.5 eq.), bis(1,5-cyclooctadiene)nickel(0) ($Ni(COD)_2$, 1650 mg, 6 mmol, 1.5 eq.), and 1,5-cyclooctadiene (COD, 0.75 mL, 6 mmol, 1.5 eq.) in anhydrous DMF/THF (60 mL/30 mL). The mixture was stirred at room temperature under a nitrogen atmosphere for three days. Then, the mixture was cooled in an ice bath, dropwise added concentrated HCl solution (15 mL), and stirred for overnight. The precipitate was collected, washed with DMF (3 × 10 mL), water (3 × 10 mL), and methanol (3 × 10 mL), respectively, and soxhlet extracted in methanol for 48 h, dried in vacuum to give off-white solids. Deprotection of *Boc* groups was performed by using 4 M HCl in methanol (10 mL) for 4 h at room temperature. After rotary evaporation, the excess HCl were removed by triturating the residue with methanol (saturated with ammonia). The solid was filtrated and soxhlet extracted in methanol for 24 h, and dried in vacuum at 80 °C for overnight to obtain **dPOF-1**–**3** (the feeding molar ratios of building blocks between **Br_2-L_1-*Boc*** and **Br_4tpm** are 1:3, 1:1 and 3:1 for **dPOF-1**, **dPOF-2** and **dPOF-3**, respectively) as off-white solids. The synthetic procedure of **dPOF-4** was the same as that for **dPOF-1** except that **Br_2-L_1-*Boc*** (0.25 mmol) was replaced by **Br-L_2-*Boc*** (0.25 mmol).

2.3. Catalytic test

Typical procedure of the asymmetric aldol reaction is described as following. To a mixture of the anhydrous solvent (4 mL) and the ketone donor (1 mL) was added the aldehyde (0.05 mmol) followed

by the catalyst (10 mol%), and the resulting mixture was stirred at room temperature for 24 h. The mixture was centrifuged, washed with ethyl acetate for three times, and the combined organic supernatant was dried over anhydrous $MgSO_4$, concentrated in rotary evaporation, and dried on vacuum overnight to get the crude product. The pure aldol products were obtained by flashed chromatography (200–300 mesh silica gel, mixture of ethyl acetate/petroleum ether = 1:4). The conversion and the diastereoselectivity were determined by ^1H NMR analysis of the crude aldol product. The enantiomeric excess value was determined by high performance liquid chromatography.

2.4. Recycle use of dPOFs

The catalysts (**dPOF-1** or **dPOF-4**) were recovered via centrifuge, washed with ethyl acetate for three times and simply dried on vacuum at 60 °C overnight before reuse.

3. Results and discussion

3.1. Design of dPOFs

To elucidate our inspiration, herein we take one of the classical POF, PAF-1 (also named PPN-6 by Zhou group) [10,26], as a model POF for explanation in details. PAF-1 was synthesized by coupling of 4-connected tetrahedral rigid building block **Br_4tpm** (Fig. 1). With the default diamondoid structure, PAF-1 has an ultrahigh surface area (S_{BET} = 5600 $m^2\ g^{-1}$) and high physicochemical stability. To date, surface function of PAF-1 can be achieved by pre-modification of the tetrahedral building block (Fig. 1a). For example, Farha, Hupp, Nguyen and their co-authors accessed five functionalized PAFs (i.e. PAF-1–CH_3, —CH_2OH, —CH_2NH_2, —CH_2-phthalimide, and —$CH_2N{=}CMe_2$) through separate coupling of the corresponding functionalized Br_4tpm building blocks [27]. The syntheses of the functionalized Br_4tpm building blocks, however, are tedious and exhaustive; more importantly, it is challenging to introduce functional groups into the 4-connected Br_4tpm building blocks. Through PSM modification, sulfonic acid, hydroxyl, alkyl and amino groups can be grafted in the pores of PAF-1 (Fig. 1b) [28,29]. Nevertheless, the pore sizes significantly decreased. For example, the pore sizes decreased from 13.6 Å for PPN-6 to 7.5 Å for sulfated framework (PPN-6-SO_3H) and 6.1 Å for lithium sulfated framework (PPN-6-SO_3Li) [26]. The PSM process was largely limited since large reagents cannot penetrate into the pores. In addition, the extent that a PAF-1 particle can be post-synthetically modified largely depends on the mass transportation of the reagents in the whole morphological structures, which may result to the uneven distribution of the functional groups since the outer "shell" would be more highly functionalized than the inner "core".

To introduce the accessible functional groups such as active catalytic sites, dPOFs could be synthesized by the copolymerization of

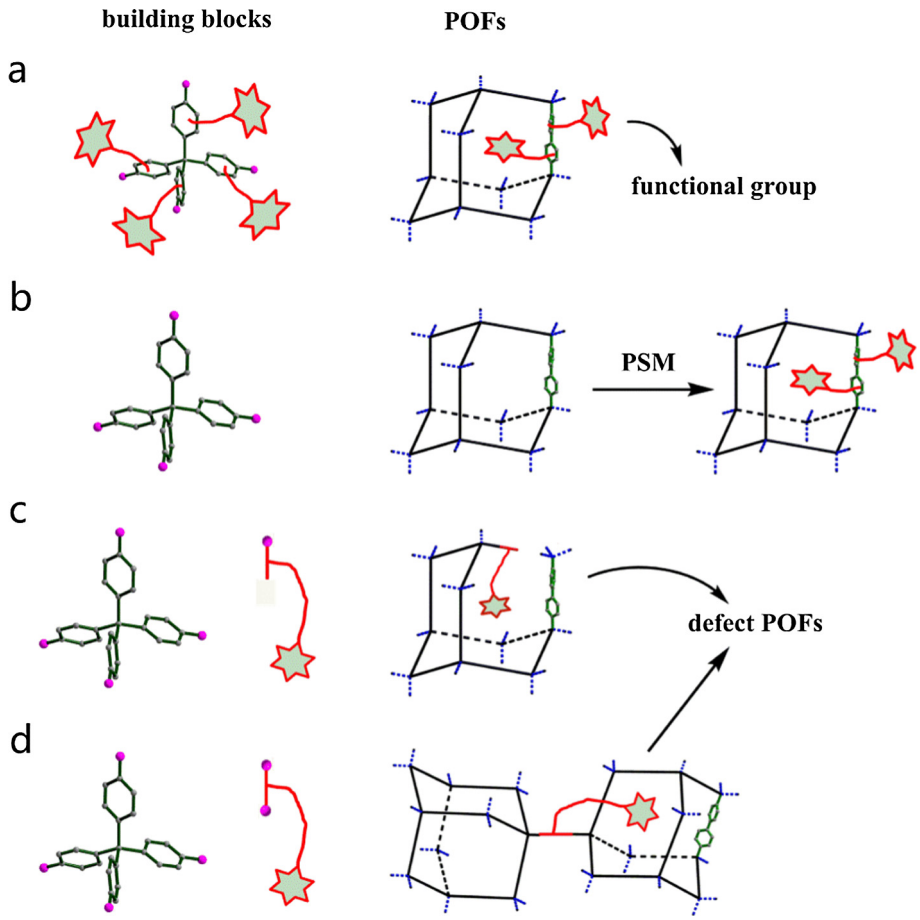

Fig. 1. Strategies for introducing functional groups into PAF-1; (a) the pre-modification process. (b) Post-synthetic modifications (PSM). dPOFs with targeted functional groups synthesized by one-pot copolymerization of the primitive tetrahedral building blocks and the low-connected such as (c) 1-connected or (d) 2-connected functional building blocks.

an appropriate amount of 1- or 2- connected functional building blocks with 4-connected tetrahedral building block Br_4tpm in the *de novo* synthesis.

The default diamondoid structure can be partially formed and located around the functional building blocks in the resulting dPOFs, which provides widely open and interconnected pores that efficiently prevent the formation of "dead space" and facilitate the accessible to the functional groups (Fig. 1c and d).

3.2. Synthetic procedure

As shown in Scheme 1a, the syntheses of proline-functionalized **dPOF-1**–**3** were carried out by the nickel(0)-catalyzed Yamamoto-type Ullmann cross-coupling reaction of the proline-functionalized 2-connected building block **Br_2-L_1-*Boc*** and the 4-connected tetrahedral building blocks **Br_4tpm**. Treating with hydrogen chloride in methanol (4 M) and subsequently treating with saturated ammonium in methanol finally obtained targeted proline-functionalized polymers **dPOF-1**–**3** (the feeding molar ratios of building blocks between **Br_2-L_1-*Boc*** and Br_4tpm were 1:3, 1:1 and 3:1 for **dPOF-1**, **dPOF-2** and **dPOF-3**, respectively). The synthetic procedure of **dPOP-4** was the same as that for **dPOP-1** except that the 2-connectd building block **Br_2-L_1-*Boc*** was replaced by the 1-connected building block **Br-L_2-*Boc*** (Scheme 1b). **dPOF-1**–**4** are insoluble in water and common organic solvents and display an excellent chemical stability since they are isolated from the harsh reaction conditions. The components of **dPOF-1**–**4** were determined by EA, and the real contents of the **L_1** or **L_2** moieties were calculated from the amount of sulfur. The results suggest that every **L_1** or **L_2** moiety was inter-connected to approximately 4.4, 2.1, 1.2 and 7.8 **tpm** moieties in **dPOF-1**, **dPOF-2**, **dPOF-3**, and **dPOF-4**, respectively.

3.3. Structural characterization

No residual bromine was observed in the as-prepared dPOFs based upon elemental analyses, indicating the efficiency of the Yamamoto cross-coupling and the completion of the reactions. The successful incorporation of **L_1** or **L_2** units was further confirmed by the N/S elemental ratios calculated from the EA results, where the experimental values are 2.50, 2.12, 2.01 and 2.07 for **dPOF-1**, **dPOF-2**, **dPOF-3**, and **dPOF-4** (Table S1), respectively. These values are slightly larger than the idealized value calculated from the **L_1** or **L_2** moieties (i.e., 2), presumably because the residue of a trace amount of 2,2′-bipyridine is occupying in the pores of dPOFs. To monitor the reaction procedures, the as-synthesized dPOFs as well as initial building blocks were studied by Fourier transform infrared (FT-IR) spectroscopy. As shown in Figs. S2 and S3, the disappearance of the two diagnostic C-Br stretching vibration absorption bands (532 cm^{-1} and 509 cm^{-1} for Br_4tpm; 513 and 495 cm^{-1} for **Br_2-L_1-*Boc***; 554 cm^{-1} and 541 cm^{-1} for **Br-L_2-*Boc***) in the as-prepared **dPOF-1**–**4** preliminarily demonstrated that most of the bromide functional group in the starting materials had been consumed by phenyl-phenyl coupling. To further reveal the local structures of the obtained polymers, solid-state ^{13}C cross-polarization magic-angle spinning nuclear magnetic resonance (CP/MAS NMR) were carried out (Fig. 2). The NMR spectra of the dPOFs were dominated by five pronounced signals at approximately 145, 139, 131, 126, and 64 ppm, which are in accordance with that of PAF-1 where the corresponding signals are 146, 140, 131, 125, and 64 ppm [10]; therefore, these five signals can be

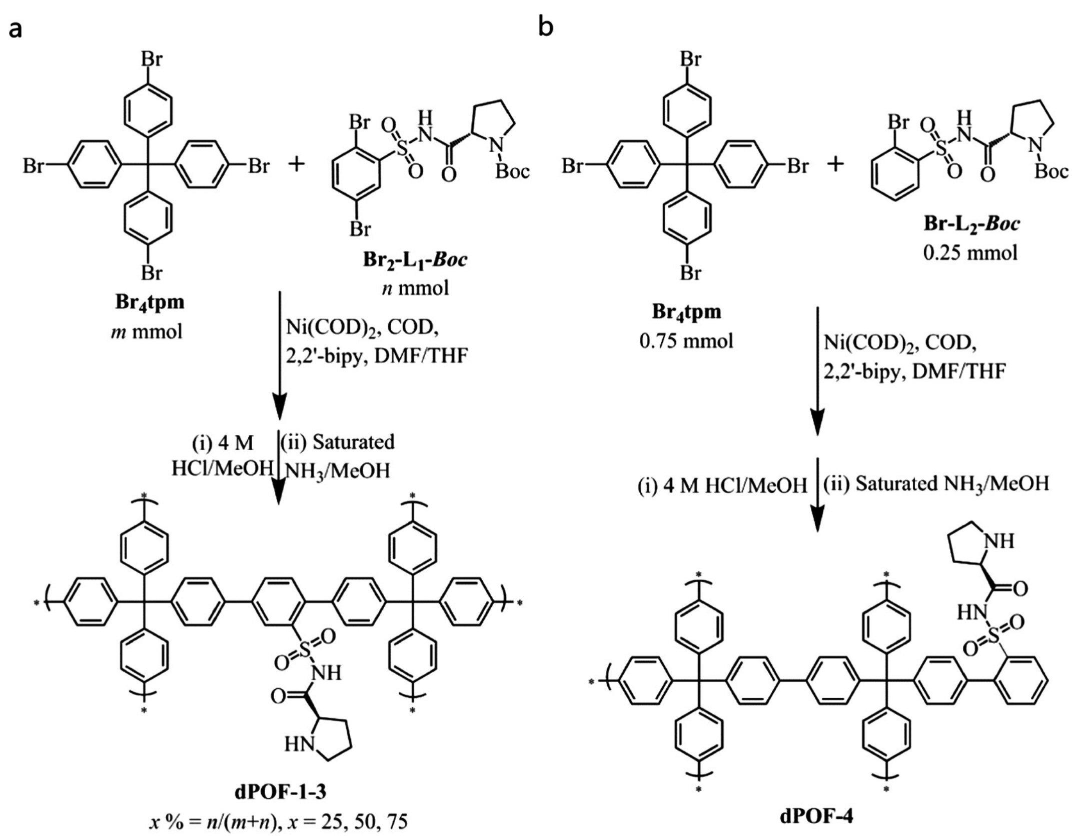

Scheme 1. The syntheses of proline-functionalized (a) dPOF-1–3 and dPOF-4.

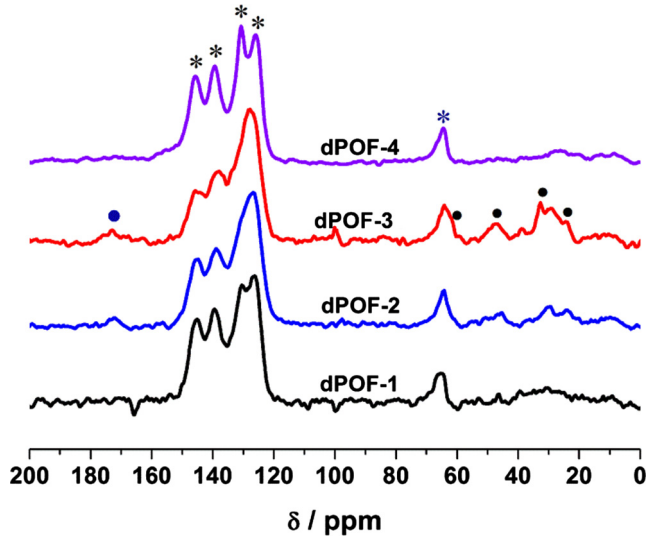

Fig. 2. ^{13}C solid-state cross-polarization magic angle spinning NMR spectra of dPOF-1–4; signals from tpm moieties (*) and proline-functionalized L_1 or L_2 moieties (•).

unambiguously assigned to the carbon atoms from the **tpm** moieties. The signal at approximately 173 ppm was assigned to the carbon atom in the carbonyl group, and the signals at approximately 47, 32 and 23 ppm were assigned to the pyrrole rings in the proline-species; these signals are strengthened by the content of $\mathbf{L_1}$ moieties increasing from **dPOF-1** to **dPOF-3**. Although the signals of some carbon atoms from the $\mathbf{L_1}$ moieties, such as the carbon atoms from the phenyl, could not be exactly assigned, the NMR spectra clearly indicated the **tpm** moieties and the functional $\mathbf{L_1}$ or $\mathbf{L_2}$ moieties are uniformly distributed in the skeleton of these dPOFs. To explore the thermal stability of dPOFs, thermogravimetric analysis (TGA) was performed under nitrogen atmosphere. Only a slight weight loss before 200 °C were observed, revealing that the high thermal stability of these dPOFs (Fig. S4). In order to probe the long-range structure of dPOFs, powder X-ray diffraction (PXRD) was performed (Fig. S5). The PXRD patterns showed that the intensity of the broad peaks at *ca.* 10, 16, and 22 deg are obviously weaken from **dPOF-1** to **dPOF-3**, which indicates that the drop of long-range order of the structures with the increase of the $\mathbf{L_1}$ moieties. Scanning electron microscopy (SEM) images of **dPOF-1–4** revealed that only spherical aggregates of small particles with sizes of 300–500 nm are observed (Fig. S6), which to some extent indicates the phase purity of these materials. Energy-dispersive X-ray spectroscopy (EDS) showed that no bromine residues remained in **dPOF-1–4** (Fig. S8), and the EDS elemental mapping displayed a homogeneous distribution of nitrogen and sulfur elements in the dPOFs (Fig. S9), both of which further indicate the good cross-coupling between the two initial building blocks.

3.4. Gas sorption measurements

To investigate the porosity of the dPOFs, the as-prepared samples of **dPOF-1–4** as well as PAF-1 were activated under dynamic vacuum at 80 °C overnight and the N_2 sorption isotherms were collected at 77 K. As shown in Fig. 3a, the resulting isotherms show type I adsorption isotherms featured by a sharp uptake at the low-pressure region. The Brunauer-Emmett-Teller (BET) surface areas obtained from experimental data are 3087, 1484, 886, 326 and 1741 $m^2\ g^{-1}$ for PAF-1, **dPOF-1**, **dPOF-2**, **dPOF-3**, and **dPOF-4**, respectively. The total pore volume obtained using the *t*-plot method is 2.66 $cm^3\ g^{-1}$ for PAF-1, 0.85 $cm^3\ g^{-1}$ for **dPOF-1**, 0.43 $cm^3\ g^{-1}$ for **dPOF-2**, 0.20 $cm^3\ g^{-1}$ for **dPOF-3** and 1.36 $cm^3\ g^{-1}$

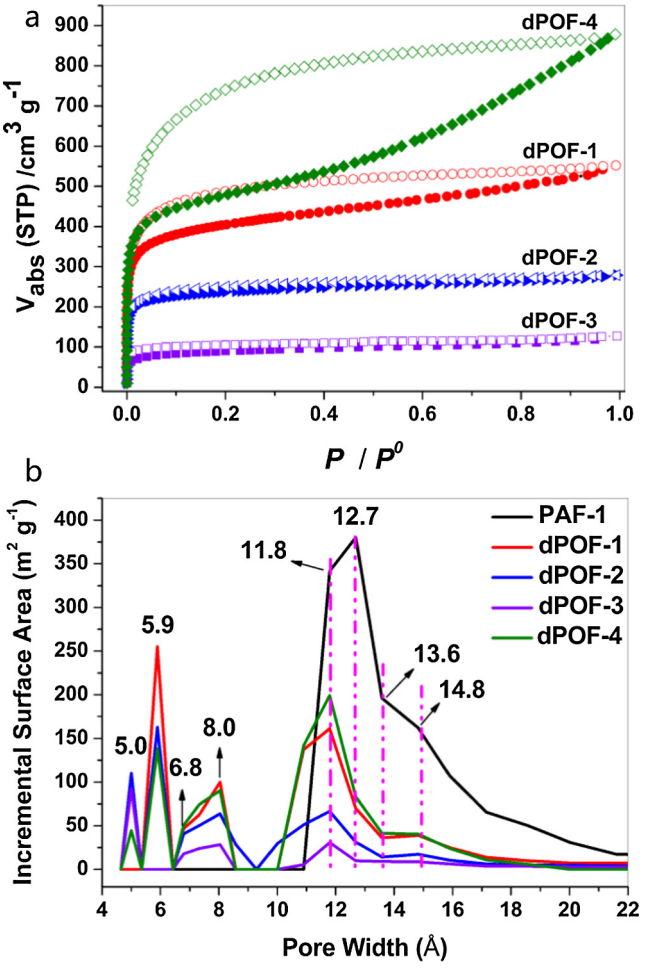

Fig. 3. N_2 sorption isotherms of dPOF-1–4 and (b) the pore size distribution of dPOF-1–4 as well as PAF-1.

for **dPOP-4**. The pore size distribution calculated from nonlinear density functional theory (NLDFT) shows that the as-synthesized PAF-1 displays a narrow distribution at approximate 11.8, 12.7, 13.6, and 14.8 Å, in accordance with that of previously reported [26]. The pore size distribution of **dPOF-1–4**, however, is distinct from that of PAF-1 (Fig. 3b). On the one hand, **dPOF-1–4** exhibit fractional pores as same as PAF-1 (i.e., 11.8, 12.7, 13.6, and 14.8 Å), indicating the presence of the default diamondoid structure in dPOFs similar to that of PAF-1; on the other hand, some small pores at approximately 8.0, 6.8, 5.9, and 5.0 Å for **dPOF-1–3** and 8.2, 7.3, 6.8, 5.9, and 5.0 Å for **dPOP-4** are also observed. Compared with PAF-1, the presence of small pores may result from the protrusion of the flexible proline-based species in the $\mathbf{L_1}$ or $\mathbf{L_2}$ moieties into the partial pores of the structure. Importantly, an appropriate feeding molar ratio of functional building blocks to primitive building blocks is vitally important to prepare targeted functional dPOFs since surface area, total pore volume, and amount of characteristic diamondoid structure progressively decrease with the increase in low-connected functional moieties.

3.5. Heterogeneous asymmetric organocatalysis

Recently, chiral organocatalysts have rapidly developed into a vital tool for the asymmetric synthesis of chiral compounds [31]. However, high loading of organocatalysts, together with laborious separation processes in homogeneous systems has generally obstructed their practical applications. One of the most promising

strategies, the so-called "immobilization" of organocatalysts, may address these problems by facilitating product separation and catalyst reuse [32]. Various supports such as linear polymers, polystyrene spheres (PS), dendrimers, and silica have been applied in the immobilization of chiral organocatalysts; nevertheless, most of these catalysts often suffer from low catalytic activities as a result of inefficient access to the catalytic sites [33]. To overcome this issue, porous metal-organic framework (MOF)-based organocatalysts have been developed [34–40]; but their low chemical stabilities limited their applications as chiral organocatalysts. With high surface areas and excellent physicochemical stability, POFs have been proposed as a very promising supports in the immobilization of organocatalysts [41,42]; however, due to the lack of facile methods to integrate the organocatalytic sites into the skeletons of a POF, only several POF-based organocatalysts have been reported so far [43–50]. We envisage that dPOFs may serve as a platform for heterogeneous chiral organocatalysis since the active catalytic sites can be readily incorporated into dPOFs.

L-Proline and its derivatives are well-known asymmetric organocatalysts, accelerating a variety of enantioselective organic reactions such as aldol reactions [30]. To evaluate the catalytic activity of **dPOF-1–3**, we selected the direct asymmetric aldol reaction between *p*-nitrobenzaldehyde and acetone as a mode reaction. Solvent screening showed that **dPOF-1** possesses the best catalytic performance in neat acetone (Table 1, Entries 1–5); with a 10 mol% **dPOF-1** loading, **dPOF-1** achieved over 99% conversion in 24 h with a maximum isolated yield of 83% and a ee value of 83.1%. Under such conditions, the catalytic performances of **dPOF-2–3** were also assessed (Table 1, Entries 5–6). Among them, **dPOF-2** resulted in a negligible difference in both conversion and isolated yield but modest enantioselectivity in comparison with **dPOF-1**, whereas **dPOF-3** exhibited the lowest catalytic activity and the modest enantioselectivity (Table 1, Entry 7). The catalytic activity and enantioselectivity decreased with an increasing density of the proline-based $\mathbf{L_1}$ species; presumably, because of the reduction in surface area and the increase in narrow pore ratios from **dPOF-1** to **dPOF-3**, decreasing the accessibility of the catalytic sites and lowering the efficiency of the mass transport. In addition, the effect of the catalyst loading was examined; when the amount of catalyst **dPOF-1** was reduced from 10 to 5 mol%, the conversation largely decreased from 99% to 56% and the isolated yield greatly decreased from 83% to 43%, while the ee value only slightly reduce from 83.1% to 79.4% (Table 1, Entry 8). Further experiments indicated that the enantioselectivity is almost independent to the amount of **dPOF-1** and reaction time (Table 1, Entries 5, 8–10). Control experiment demonstrated that the parent framework itself (PAF-1) is completely inactive, indicating that the proline-based $\mathbf{L_1}$ species are responsible for the observed catalytic activity (Table 1, Entry 11). Noticeably, the removal of **dPOF-1** catalyst by centrifugation after 5 h almost completely shut down the reaction, affording only 3.6% additional conversion and almost the same isolated yield and ee value after stirring for another 19 h, indicating that no leaching of catalytically active species and the intrinsic heterogeneous nature of catalyst **dPOF-1** (Table 1, Entry 12). The heterogeneous catalyst **dPOF-1** has significantly higher catalytic activity but slightly lower ee value than its homogeneous acylsulfonamide catalyst ((*S*)-N-(2,5-dibromophenylsulfonyl)pyrrolidine-2-carboxamide, $\mathbf{Br_2\text{-}L_1}$) (Table 1, Entry 13); the higher activity may be attributed to the uniform distribution of the proline-based $\mathbf{L_1}$ species towards the pores of **dPOF-1**, while the slightly lower enantioselectivity presumably originates from the restricted movement of the substrates on the small pores of **dPOF-1**. Remarkably, the catalysts **dPOF-1, dPOF-2** and **dPOF-4** showed both higher activity and better enantioselectivity than that of another homogeneous L-proline counterpart, even when 20 mol% L-proline was used under the optimized reaction conditions previously reported by List et al. (Table 1, Entries 14–16) [30].

Using the optimized reaction conditions, the substrate scope of the direct asymmetric aldol reaction of ketones with nitrobenzaldehyde was investigated, and the results are summarized in Table 2. As depicted in Table 2, the as-prepared **dPOF-1** could well catalyze the direct asymmetric aldol reactions between nitrobenzaldehyde and acetone, cyclopentanone and cyclohexanone with excellent isolated yields (71–83%) and enantioselectivity (ee 66–85%). When butanone was employed as the ketone, only modest isolated yields (30–34%) of the corresponding 1-hydroxy-1-(nitrophenyl)pentan-3-one were obtained because another condensation product, 4-hydroxy-3-methyl-4-(nitrophenyl)butan-2-one,

Table 1
Optimization of the reaction of 4-nitrobenzaldehyde with acetone.[a]

Entry	Solvent	Catalyst	Catalyst loading (mol%)	Time (h)	Conversion[b] (%)	Yield[c] (%)	ee[d] (%)
1	DMSO	dPOF-1	10	24	55	43	86.6
2	Methanol	dPOF-1	10	24	39	23	59.1
3	Acetonitrile	dPOF-1	10	24	52	42	74.7
4	DCM	dPOF-1	10	24	55	47	79.2
5	Acetone	dPOF-1	10	24	>99	83	83.1
6	Acetone	dPOF-2	10	24	98	85	77.8
7	Acetone	dPOF-3	10	24	89	64	74.2
8	Acetone	dPOF-1	5	24	56	43	79.4
9	Acetone	dPOF-1	10	5	59.8	44	79.8
10	Acetone	dPOF-1	10	15	83.7	62	80.3
11	Acetone	PAF-1	10	24	0	0	–
12[e]	Acetone	dPOF-1	10	5	63.4	44	79.0
13	Acetone	Br_2-L_1	10	24	>99	35	92.7
14	Acetone	L-proline	10	24	>99	40	47.9
15	DMF	L-proline	20	24	>99	65 68[f]	74.5 76[f]
16	Acetone	dPOF-4	10	24	>99	78	83.6

[a] Typically, the reactions were performed with 4-nitrobenzaldehyde (76 mg, 0.5 mmol), acetone (1 mL) and catalyst (1–10 mol%) in corresponding solvents (4 mL, 80 vol%) at room temperature.
[b] Determined by ^{1}H NMR of the crude product.
[c] Isolated yields after column chromatography.
[d] Determined by HPLC on chiral columns.
[e] The supernatant was stirred in inert atmosphere for another 19 h.
[f] Reported by the Ref. [30].

Table 2
Results of reaction of various ketones with nitrobenzaldehyde.[a]

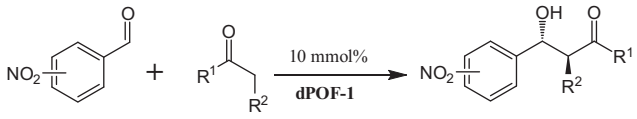

Entry	Substrate	R^1	R^2	Isolated yield[b] (%)	*syn*/*anti*[c]	ee[d] (%)
1	4-NO_2	Me	H	83	–	83.1
2	3-NO_2	Me	H	75	–	84.3
3	2-NO_2	Me	H	73	–	83.1
4	4-NO_2	Et	H	30	–	72.6
5	2-NO_2	Et	H	34	–	85.5
6	4-NO_2	$-(CH_2)_3-$		74	49/51	66.4[e]
7	3-NO_2	$-(CH_2)_3-$		73	48/52	84.7[e]
8	2-NO_2	$-(CH_2)_3-$		74	37/63	84.8[e]
9	4-NO_2	$-(CH_2)_4-$		71	27/73	74.9[e]

[a] Typically, the reactions were performed with catalyst (**dPOF-1**, 10 mol%) and corresponding aldehyde (0.5 mmol) in neat ketone (5 mL) for 24 h at room temperature.
[b] Combined yields of isolated diastereomers.
[c] Determined by NMR spectra of the isolated products.
[d] Determined by chiral-phase HPLC analysis.
[e] The anti product.

was competitively generated. The porous materials based on heterogeneous organocatalysts for the aldol reaction reported to date were summarized in Table S4. Among them, **dPOF-1** is one of the heterogeneous chiral organocatalysts with the highest catalytic activity and best enantioselectivity.

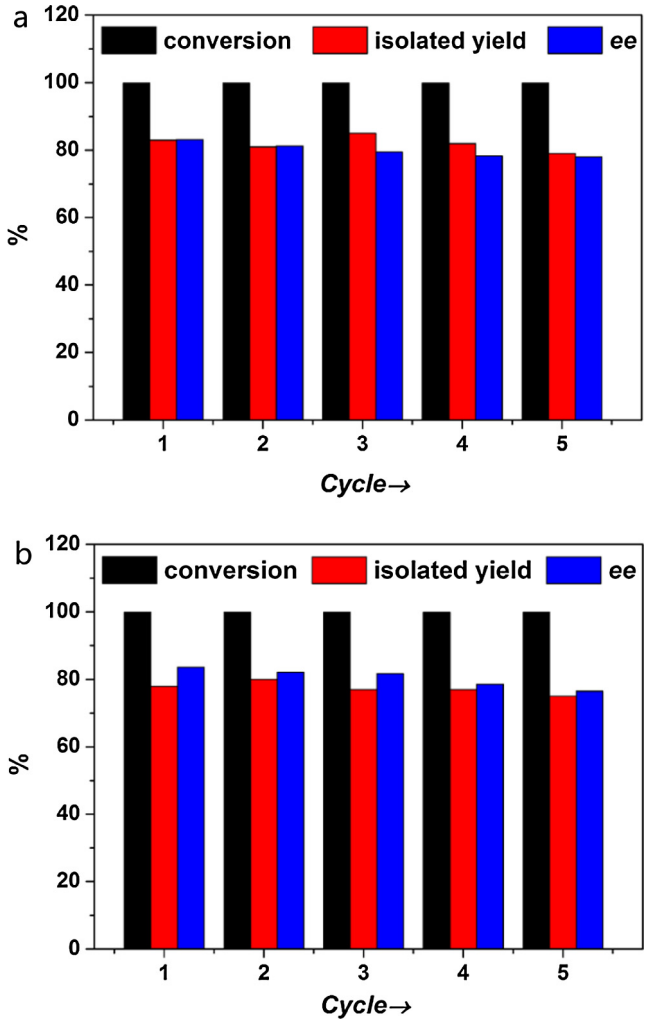

Fig. 4. The recycled experiment of (a) dPOF-1 and (b) dPOF-4.

The recyclability of the dPOFs catalysts was assessed by using **dPOF-1** and **dPOF-4** as model organocatalysts and employing the direct aldol reaction of 4-nitrobenzaldehyde with acetone as a model reaction. **dPOF-1** and **dPOF-4** can be readily isolated from the reaction suspension by simple centrifugation. The recycled solids could be reused at least five runs with the retention of their catalytic activities and only a slight decrease in enantioselectivities, which could be attributed to the covalent anchoring of catalytically active sites as well as framework robustness (Fig. 4, and Tables S2 and S3). Only a slightly reduction in surface areas and no obvious change of the pore sizes were observed for recycled **dPOF-1** and **dPOF-4**, even after five catalytic runs (Figs. S10–S13). Moreover, SEM images showed that the recycled **dPOF-1** and **dPOF-4** could well retain their spherical shapes (Fig. S14). These results show that **dPOF-1** and **dPOF-4** could well retain their structural integrity after five catalytic runs.

4. Conclusion

In summary, we developed a facile and versatile strategy to construct dPOFs facilitating to immobilization of targeted functional groups by copolymerization of an appropriate amount of low-connected such as 1- or 2-connected functional and primitive multi-connected building blocks in the *de novo* synthesis. Based on this strategy, **dPOF-1**–**4** ligated with proline-functionalized groups were readily built. The as-synthesized dPOFs showed high chemical stability, high porosity and excellent guest-molecule accessibility due to the present of diamondoid structure neighboring the functional groups in their skeletons. Serving as a heterogeneous chiral organocatalyst, **dPOF-1** shows outstanding performances in the catalytic direct asymmetric aldol reactions. Remarkably, **dPOF-1**, **dPOF-2**, and **dPOF-4** display higher catalytic activity and superior enantioselectivity than those of their homogeneous L-proline counterpart in the direct asymmetric aldol reactions between 4-nitrobenzaldehyde and acetone, and these heterogeneous dPOFs-based chiral organocatalysts could be reused for at least five times without significant loss of catalytic activity and enantioselectivity. Our strategy may thus facilitate the design of targeted functional dPOFs combining of permanent porosity and functional groups accessibility and would greatly extend the applications of POFs.

Acknowledgements

This work was financially supported by the 973 Program (2014CB845605), NSFC (21521061, 21331006, 21520102001, 21303205 and 21571177), the "Strategic Priority Research Program" of the Chinese Academy of Sciences (XDA09030102), Fujian Agriculture and Forestry University (118360020), Outstanding Youth Research Training Program of Fujian Agriculture and Forestry University (XJQ201616), and the State Key Laboratory of Structural Chemistry, Fujian Institute of Research on the Structure of Matter, Chinese Academy of Sciences (20170028).

Appendix A. Supplementary material

Supplementary data associated with this article can be found, in the online version, at https://doi.org/10.1016/j.jcat.2017.09.014.

References

[1] Y. Xu, S. Jin, H. Xu, A. Nagai, D. Jiang, Chem. Soc. Rev. 42 (2013) 8012.
[2] P.J. Waller, F. Gándara, O.M. Yaghi, Acc. Chem. Res. 48 (2015) 3053.
[3] S. Lin, C.S. Diercks, Y.-B. Zhang, N. Kornienko, E.M. Nichols, Y. Zhao, A.R. Paris, D. Kim, P. Yang, O.M. Yaghi, C.J. Chang, Science 349 (2015) 1208.
[4] Y. Liu, Y. Ma, Y. Zhao, X. Sun, F. Gandara, H. Furukawa, Z. Liu, H. Zhu, C. Zhu, K. Suenaga, P. Oleynikov, A.S. Alshammari, X. Zhang, O. Terasaki, O.M. Yaghi, Science 351 (2016) 365.
[5] E. Rozhko, A. Bavykina, D. Osadchii, M. Makkee, J. Gascon, J. Catal. 345 (2017) 270.
[6] K. Wang, Z. Jia, X. Yang, L. Wang, Y. Gu, B. Tan, J. Catal. 348 (2017) 168.
[7] P. Kuhn, M. Antonietti, A. Thomas, Angew. Chem., Int. Ed. 47 (2008) 3450.
[8] J.-X. Jiang, F. Su, A. Trewin, C.D. Wood, N.L. Campbell, H. Niu, C. Dickinson, A.Y. Ganin, M.J. Rosseinsky, Y.Z. Khimyak, A.I. Cooper, Angew. Chem., Int. Ed. 46 (2007) 8574.
[9] P.M. Budd, B.S. Ghanem, S. Makhseed, N.B. McKeown, K.J. Msayib, C.E. Tattershall, Chem. Commun. (2004) 230.
[10] T. Ben, H. Ren, S. Ma, D. Cao, J. Lan, X. Jing, W. Wang, J. Xu, F. Deng, J.M. Simmons, S. Qiu, G. Zhu, Angew. Chem., Int. Ed. 48 (2009) 9457.
[11] D. Yuan, W. Lu, D. Zhao, H.-C. Zhou, Adv. Mater. 23 (2011) 3723.
[12] X. Zou, H. Ren, G. Zhu, Chem. Commun. 49 (2013) 3925.
[13] S. Dalapati, M. Addicoat, S. Jin, T. Sakurai, J. Gao, H. Xu, S. Irle, S. Seki, D. Jiang, Nat. Commun. 6 (2015) 7786.
[14] X. Zhang, C. Wang, P. Wang, J. Du, G. Zhang, L. Pu, Chem. Sci (2016).
[15] H. Zhong, C. Liu, Y. Wang, R. Wang, M. Hong, Chem. Sci. 7 (2016) 2188.
[16] N. Huang, R. Krishna, D. Jiang, J. Am. Chem. Soc. 137 (2015) 7079.
[17] W.-K. An, M.-Y. Han, C.-A. Wang, S.-M. Yu, Y. Zhang, S. Bai, W. Wang, Chem.-Eur. J. 20 (2014) 11019.
[18] N. Huang, X. Chen, R. Krishna, D. Jiang, Angew. Chem., Int. Ed. 54 (2015) 2986.
[19] A. Nagai, Z. Guo, X. Feng, S. Jin, X. Chen, X. Ding, D. Jiang, Nat. Commun. 2 (2011) 536.
[20] E. Verde-Sesto, M. Pintado-Sierra, A. Corma, E.M. Maya, J.G. de la Campa, M. Iglesias, F. Sánchez, Chem.-Eur. J. 20 (2014) 5111.
[21] T. Ratvijitvech, R. Dawson, A. Laybourn, Y.Z. Khimyak, D.J. Adams, A.I. Cooper, Polymer 55 (2014) 321.
[22] Z. Fang, B. Bueken, D.E. De Vos, R.A. Fischer, Angew. Chem., Int. Ed. 54 (2015) 7234.
[23] M. Taddei, Coord. Chem. Rev. 343 (2017) 1.
[24] H. Wu, Y.S. Chua, V. Krungleviciute, M. Tyagi, P. Chen, T. Yildirim, W. Zhou, J. Am. Chem. Soc. 135 (2013) 10525.
[25] J. Park, Z.U. Wang, L.-B. Sun, Y.-P. Chen, H.-C. Zhou, J. Am. Chem. Soc. 134 (2012) 20110.
[26] W. Lu, D. Yuan, J. Sculley, D. Zhao, R. Krishna, H.-C. Zhou, J. Am. Chem. Soc. 133 (2011) 18126.
[27] S.J. Garibay, M.H. Weston, J.E. Mondloch, Y.J. Colon, O.K. Farha, J.T. Hupp, S.T. Nguyen, CrystEngComm 15 (2013) 1515.
[28] W. Lu, J.P. Sculley, D. Yuan, R. Krishna, Z. Wei, H.-C. Zhou, Angew. Chem., Int. Ed. 51 (2012) 7480.
[29] C. Pei, T. Ben, S. Qiu, Mater. Horiz. 2 (2015) 11.
[30] B. List, R.A. Lerner, C.F. Barbas, J. Am. Chem. Soc. 122 (2000) 2395.
[31] D.-F. Chen, Z.-Y. Han, X.-L. Zhou, L.-Z. Gong, Acc. Chem. Res. 47 (2014) 2365.
[32] M. Bartók, Catal. Rev. 57 (2015) 192.
[33] M. Benaglia, A. Puglisi, F. Cozzi, Chem. Rev. 103 (2003) 3401.
[34] J. Canivet, S. Aguado, G. Bergeret, D. Farrusseng, Chem. Commun. 47 (2011) 11650.
[35] D.J. Lun, G.I.N. Waterhouse, S.G. Telfer, J. Am. Chem. Soc. 133 (2011) 5806.
[36] A.L.W. Demuynck, M.G. Goesten, E.V. Ramos-Fernandez, M. Dusselier, J. Vanderleyden, F. Kapteijn, J. Gascon, B.F. Sels, ChemCatChem 6 (2014) 2211.
[37] M. Yoon, R. Srirambalaji, K. Kim, Chem. Rev. 112 (2012) 1196.
[38] J. Hajek, M. Vandichel, B. Van de Voorde, B. Bueken, D. De Vos, M. Waroquier, V. Van Speybroeck, J. Catal. 331 (2015) 1.
[39] C. Zhu, Q. Xia, X. Chen, Y. Liu, X. Du, Y. Cui, ACS Catal. 6 (2016) 7590.
[40] Q. Xia, Z. Li, C. Tan, Y. Liu, W. Gong, Y. Cui, J. Am. Chem. Soc. 139 (2017) 8259.
[41] P. Kaur, J.T. Hupp, S.T. Nguyen, ACS Catal. 1 (2011) 819.
[42] Y. Zhang, S.N. Riduan, Chem. Soc. Rev. 41 (2012) 2083.
[43] D.S. Kundu, J. Schmidt, C. Bleschke, A. Thomas, S. Blechert, Angew. Chem., Int. Ed. 51 (2012) 5456.
[44] C.A. Wang, Z.K. Zhang, T. Yue, Y.L. Sun, L. Wang, W.D. Wang, Y. Zhang, C. Liu, W. Wang, Chem.-Eur. J. 18 (2012) 6718.
[45] J. Schmidt, D.S. Kundu, S. Blechert, A. Thomas, Chem. Commun. 50 (2014) 3347.
[46] H. Xu, X. Chen, J. Gao, J. Lin, M. Addicoat, S. Irle, D. Jiang, Chem. Commun. 50 (2014) 1292.
[47] H. Xu, J. Gao, D. Jiang, Nat. Chem. 7 (2015) 905.
[48] X. Wang, X. Han, J. Zhang, X. Wu, Y. Liu, Y. Cui, J. Am. Chem. Soc. 138 (2016) 12332.
[49] X. Han, Q. Xia, J. Huang, Y. Liu, C. Tan, Y. Cui, J. Am. Chem. Soc. 139 (2017) 8693.
[50] J. Zhang, X. Han, X. Wu, Y. Liu, Y. Cui, J. Am. Chem. Soc. 139 (2017) 8277.